Int. J. Electrochem. Sci., 14 **(2019)** 6394 – 6405, doi: 10.20964/2019.07.55

International Journal of ELECTROCHEMICAL SCIENCE
www.electrochemsci.org

Corrosion Performance of as-rolled Mg-8Li-xAl Alloys

Zilong Zhao[1,2], Yihao Li[1,2], Yifeng Zhong[1,2,], Yiding Liu[1,2],*

[1] School of Civil Engineering, Chongqing University, Chongqing 400045, China
[2] Key Laboratory of New Technology for Construction of Cities in Mountain Area (Chongqing University), Ministry of Education, Chongqing 400045, China
[*]E-mail: zhongjy58@sina.com

Received: 15 January 2019 / *Accepted:* 10 May 2019 / *Published:* 10 June 2019

In this paper, corrosion performance of Mg-8Li-xAl alloys (Mg-8Li, Mg-8Li-2Al, Mg-8Li-3Al, Mg-8Li-4Al, wt.%) in different corrosive environments were investigated by means of Scanning electron microscope (SEM), Energy-dispersive X-ray spectroscopy (EDS) and Electrochemical impedance spectroscopy (EIS). The microstructure of alloys were studies before and after the corrosion in the air and the hydrogen evolution performance in NaCl solution. The influence of elemental Al on the corrosion resistance of the alloy is revealed. When the Al content exceeds 3%, the corrosion resistance of Mg-8Li alloy in air can be obviously improved. Meanwhile, the corrosion resistance of the alloy is continuously declining in NaCl solution with the increase of aluminum content.

Keywords: Mg-8Li-xAl alloys, microstructure, hydrogen evolution, corrosion, EIS

1. INTRODUCTION

Magnesium (Mg) alloys, the lightest structural metal in the world, are considered as a potential alternative to other metallic structural engineering materials [1-3]. Mg alloys have low density, which is about two-third of that of aluminum and a quarter of that of iron. Mg alloys have lots of properties, such as high specific strength and stiffness, good damping property, outstanding heat conduction and conductivity, remarkable electromagnetic shielding performance and easy to recycle, etc. Due to these properties, Mg and Mg alloys are regarded as the “Green engineering materials in twenty-first Century” [4-6]. Many researchers are looking for effective reinforcing phases in magnesium alloys to achieve higher performance and wider application. [7, 8]. However, Mg alloys are chemical and electrochemical activity. Due to the poor corrosion resistance of magnesium alloys, it has hindered the wide application in different industries. [9]. Therefore, improving the corrosion resistance of Mg alloys has become a key research topic in Mg alloys around the word [10, 11].

Up to now, methods of anodization, conversion coating, electroplating and vapor deposition have

been put forward to improve the corrosion resistance of magnesium alloys. [12-14]. In recent studies, Zeng et al. [15] adopted a new method to prepare Zn-Al Layered Double Hydroxide (LDH) film on the surface of AZ31 by controlling the pH and temperature of the reaction solution. The results show that the obtained films can be well adhered to the magnesium matrix. The similar method was also employed in manufacturing ZnAl LDH film on the AZ91 substrate [16]. Currently, there are two main methods to prepare LDH films: (i) the in-situ method, and (ii) the co-precipitation method [17,18].

Mg Li alloy is by far the lightest nontoxic metal material. Recently, the research of MgLi alloy has become a hot topic, which has aroused extensive interest of researchers. [19-22]. Zhao et al. reported the effects of aluminum and silicon additions on the microstructure and mechanical properties of Mg4Li and Mg8Li alloy [23,24]. Xu et al. reported the superior corrosion resistance of Mg-Li alloys in the corrosive environment is believed to be accounted for a uniform lithium carbonate thin film, whereby the surface coverage is much larger than the hexagonal close-packed Mg-based alloys [25]. However, the corrosion resistance of Al-added Mg-8Li alloy and the effect of Al addition on the corrosion resistance of the alloys have rarely been reported. In this paper, the microstructure of Mg-8Li-x(0,2,3,4)Al alloys before and after the corrosion in the air and the hydrogen evolution performance in NaCl solution have been studied. Besides, the corrosion mechanism of Mg-8Li-xAl is discussed.

2. EXPERIMENTAL PROCEDURES

In this experiment, the magnetic levitation (Maglev) vacuum high frequency induction heating method was used. During casting, the materials were protected in an atmosphere of argon and cooled rapidly in a water-cooled copper crucible. Pure magnesium (purity > 99.99 wt%), pure lithium (purity > 99.9 wt%) and pure Al (purity > 99.99 wt%) were used. To ensure appropriate cleanliness, the surfaces of all pure metal and AlSi eutectic alloy ingots were scratched and ground to remove surface oxide before melting. Four alloys with nominal compositions Mg-8Li, Mg-8Li-2Al, Mg-8Li-3Al-Si and Mg-8Li-4Al-Si (weight percent) were obtained. The dimensions of the cast ingots were Ø30×60 (mm), theingots were then cut intoplates of Ø30×10 (mm). The plates were heated to 300 °C for 1 h before being subjected to the rolling process. Both the upper and lower rollers were preheated to 150 °C. The rolling reduction per pass was ~20%. A final thickness of ~1.6 mm was reached after multi-pass rolling.

Four as-rolled-annealed samples (1.6×5×10 mm) were rinsed with water, and then naturally air-dried for corrosion reaction experiments. Four as-rolled-annealed samples (20×20 mm) hydrogen evolution corrosion test was carried out with 3.5% NaCl solution. Free immersion testing without external potential was performed in 3.5 wt% NaCl solution. All the test solutions were prepared by laboratory grade reagent and deionized water. Solutions were not de-aerated, and 350 mL of NaCl solution was used in each test. The microstructure and composition were examined using a MIRA3 scanning electron microscope (SEM, Nova 400 FEI, USA) equipped with an Oxford X-ray energy dispersive spectroscopy detector (EDS INCA Energy 350 Oxford, UK).

Electrochemical Impedance Spectroscopy (EIS) were obtained at room temperature in 3.5 wt% NaCl solution using CIMPS-2 Zahner. The classical three electrode system was used as the working electrode (1 cm^2), a saturated calomel electrode (SCE) as reference electrode and platinum plate as

counter electrode. Impedance measurements were swept by a 10 mV rms sinusoidal perturbation and performed at open circuit potential (OCP) from 10 mHz to 100 kHz, with 10 experimental points collected per frequency decade above 66 Hz and 5 experimental points collected per frequency decade below 66 Hz. Zview software is used to fit the impedance diagram with different equivalent circuits. All polarization and EIS tests were performed at room temperature. There are three parallel samples in each system to ensure the importance. Potentiodynamic polarization tests were performed with a scan rate of 0.5 Mv s^{-1} over a potential range from – 1.9 V *vs.* SCE. The samples were immersed into 3.5 wt.% NaCl solution at 25 ± 1℃ for 45 min before PDP tests.

3. RESULTS AND DISCUSSION

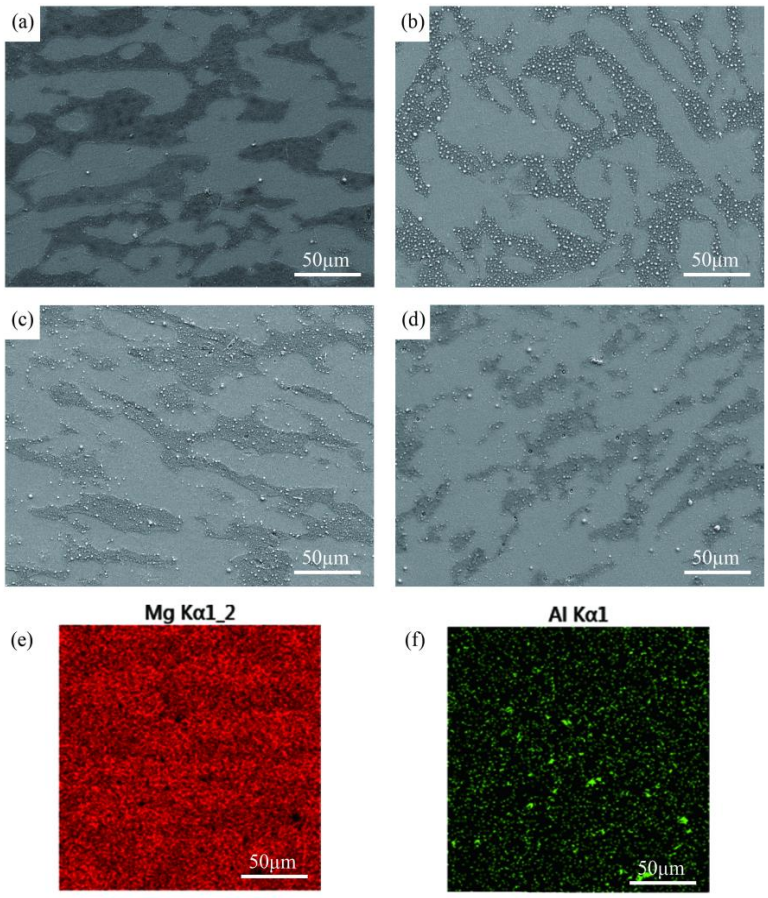

Figure 1. SEM images and EDS mappings of as-rolled Mg-8Li-xAl alloys: (a) Mg-8Li (b) Mg-8Li-2Al; (c) Mg-8Li-3Al; (d) Mg-8Li-4Al; (e and f) Mg-8Li-3Al, EDS maps.

Fig.1 shows SEM images and EDS of as-rolled Mg-8Li-xAl alloy. The Mg-8Li-xAl alloys was composed of α-phase and β-phase, whereby the light gray phase is the α phase and the dark gray phase is the β phase. No obvious precipitate phase is observed in Fig. 1a. In the Mg-8Li-2Al alloy, many precipitate phases was found, mainly precipitating in the β phase. With the increase of Al content, There are more precipitates in Mg-8Li-3Al alloy, which are precipitated in both α-phase and β-phase regions. It is indicated that the precipitation phase is first precipitated in the region of β-phase. When the Al content is 4 wt%, both the α-phase and β-phase regions have a large number of precipitation phases, with

the precipitate phase in the α-phase region continuing to increase. Fig. 1e and Fig. 1f are EDS scan maps of Mg-8Li-3Al. The precipitate phase is Al rich. According to the literature [26], the precipitate phase is the AlLi phase.

Fig. 2 shows magnified SEM images of Mg-8Li-xAl alloys. The precipitation phase of the alloy surface is further characterized under high magnification, which is consistent with the observed precipitation rule at low magnification. Reference[24] reports that the addition of Al can precipitate a particulate Al-rich phase on the α-phase region. Fig. 2 further proves that the precipitated particles in the Mg-8Li-xAl Alloy preferentially precipitate in the β-phase region. The bright white particles are not oxidized, and the dark color is oxidized during the sample preparation. Besides, the effect of this Precipitation rule on the corrosion resistance of alloys will be discussed in the following study.

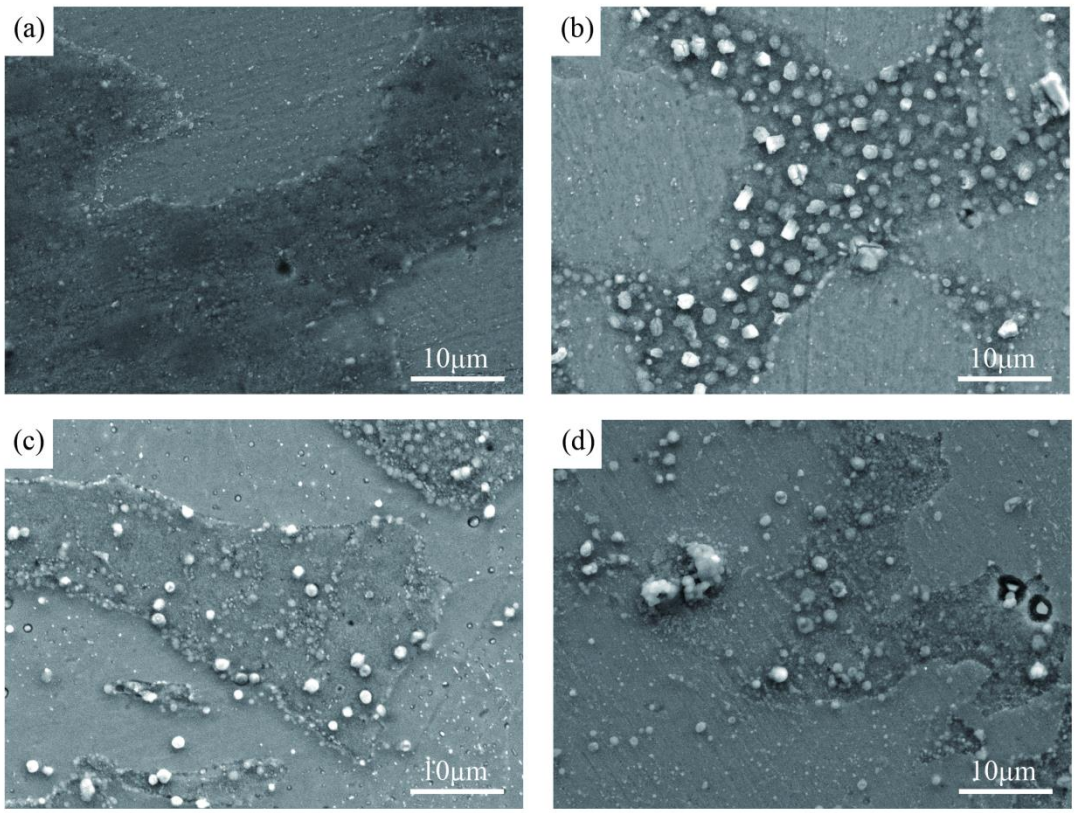

Figure 2. SEM images of as-rolled Mg-8Li-xAl alloys (a) Mg-8Li, 5K (b) Mg-8Li-2Al, 5K (c) Mg-8Li-3Al, 5K (d) Mg-8Li-4Al, 5K

Fig.3 shows the SEM and EDS images of as-rolled Mg-8Li-xAl alloys after the corrosion in the air. With the increase of Al content, the morphology of the alloy surface undergo a great change from a bird's nest-like MgO film to a smooth Al2O3 film. Fig.3a are SEM and EDS images of Mg-8Li alloy. A uniform bird nest oxide film formed on the surface of Mg-8Li alloy. The O and Mg contents are 69.43 wt% and 30.57 wt%, respectively. The surface of Mg-8Li alloy is a single MgO membrane, which separates the alloy matrix from the air and has strong corrosion resistance in the air. Fig.2b are SEM images of Mg-8Li-2Al alloy.The alloy surface is covered by bird nest film and smooth lamellar film. The O, Mg and Al contents are 77.1 wt.%, 30.57 wt.% and 0.11 wt%, respectively, It is further shown that the surface of the alloy is composed of MgO and Al2O3 nested. The increase in O content is due to

the fact that the interface between the two membranes does not protect the alloy well.

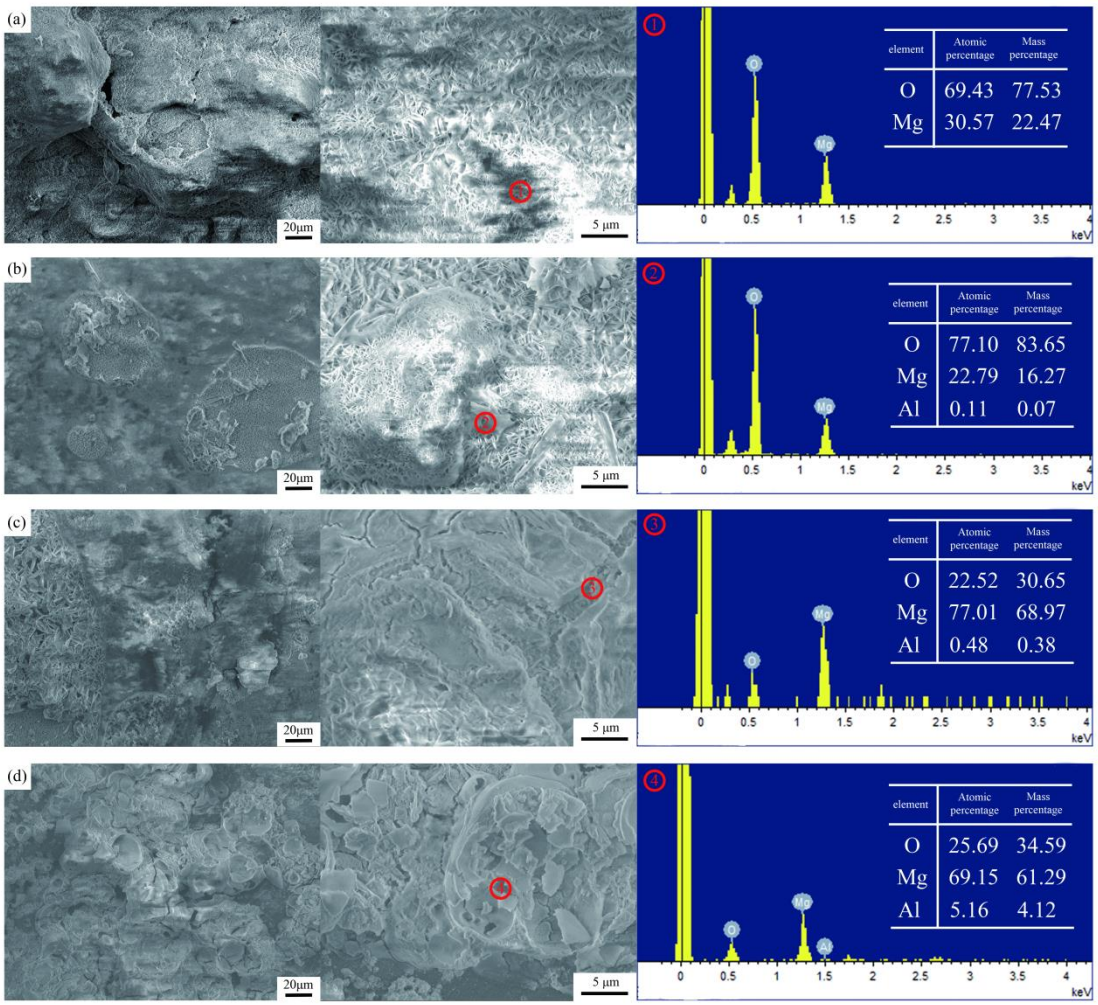

Figure 3. SEM images and EDS spectra of as-rolled Mg-8Li-xAl after the corrosion in the air for 3 days:(a) Mg-8Li (b) Mg-8Li-2Al (c)Mg-8Li-3Al (d) Mg-8Li-4Al

With the increase of Al content, it can be seen from Fig. 3c that the smooth Al2O3 surface is more in the Mg-8Li-3Al alloy. The O, Mg and Al contents are 22.52 wt%, 77.01 wt% and 0.48 wt%, respectively. Al2O3 is a denser, high temperature protective film, covering the surface of MgO, which greatly improves the corrosion resistance of magnesium alloys in air. When the Al content is 4 wt%, it can be seen from Fig.3d that almost no nested MgO is observed on the surface of the Mg-8Li-4Al alloy. All the samples are smooth and consist of Al2O3 films. The O, Mg and Al contents are 25.69 wt%, 69.15 wt% and 5.16 wt%, respectively. The above analysis shows that when the Al content exceeds 3%, the corrosion resistance of Mg-8Li alloy in air can be obviously improved.

Hydrogen evolution curves of Mg-8Li, Mg-8Li-2Al, Mg-8Li-3Al and Mg-8Li-4Al are shown in Fig.4. As can be seen from the figure, the rate of hydrogen evolution of Mg-8Li alloy increases after adding Al. With the increase of Al content, the hydrogen evolution rate of alloys become faster. In the first 15 minutes, the hydrogen evolution rate of the four alloys increases with the time flow, and the

hydrogen evolution rate of each alloy keeps at a relatively steady value after 15 minute. Mg-8Li has the lowest hydrogen evolution rate (0.1 ml/cm2 per minute), indicating that Mg-8Li has the best resistance NaCl solution corrosion. With the increase of Al content, the hydrogen evolution of Mg-8Li-2Al、Mg-8Li-3Al and Mg-8Li-4Al significantly increased, become about 0.17 ml/cm2, 0.29 ml/cm2, 0.4 ml/cm2, respectively. Xu et al. reported that more corrosion points will be formed after Al alloying [26], resulting in corrosion resistance deterioration. The addition of Al resulted in more electrochemical corrosion of Mg-8Li alloy in NaCl% solution, which accelerated the rate of hydrogen evolution.

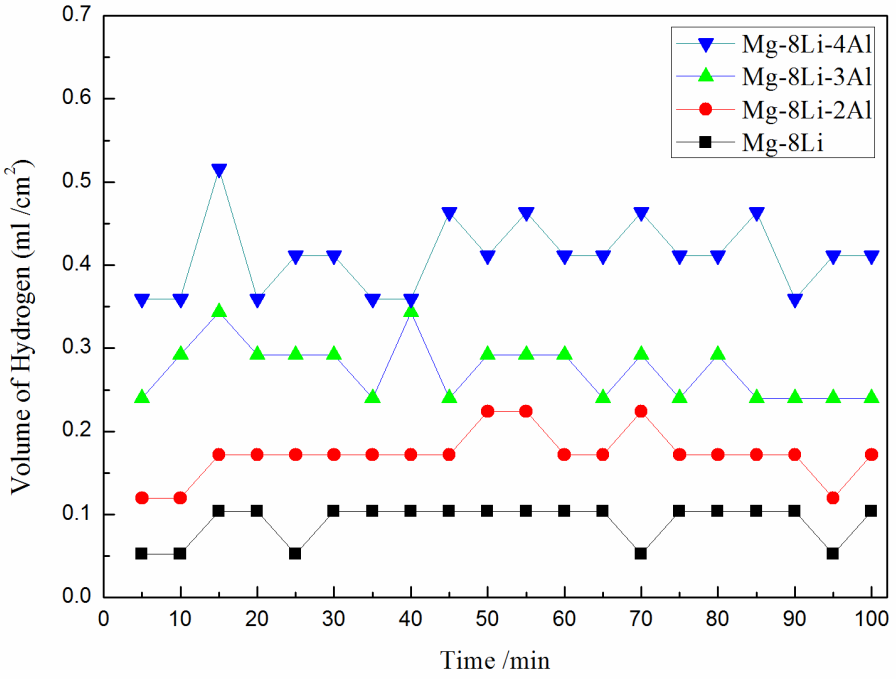

Figure 4. Hydrogen evolution curves of the as-rolled Mg-8Li-xAl alloys immersion in 3.5 wt% NaCl solution for 100 min

Fig.5 shows the SEM images of the as-rolled Mg-8Li-xAl alloys after hydrogen evolution. From Fig.5a and Fig.5b, it can be seen that the surface of Mg-8Li alloy is homogeneous after hydrogen evolution, and the corrosion products are uniformly granular, which is confirmed to be MgO [27-28]. Comparing Figs. 5a, 5c, 5e, 5f, it can be noticed that as the crack on the surface of the Mg-8Li-xAl alloy after hydrogen evolution significantly increases with the increasing content of Al. This is because the addition of Al leads to the formation of electrochemical corrosion point. The AlLi phase and Mg in the NaCl solution will electrochemically react and accelerate the rate of hydrogen evolution reaction. Therefore, cracks will appear in the area where the reaction is severe. Comparing to Figs. 5b, 5d, 5f, 5g, it can be seen that the hydrogen evolution products gradually change from a uniform distribution to an inhomogeneous distribution after a vigorous reaction. This is due to the formation of Al2O3 in AlLi position, and the formation of uniform MgO at the rest. because of the strong electrochemical reaction of Li, the formation of cracks in AlLi position. With the increase of Al content, AlLi is more and more, and the rate of hydrogen evolution reaction will accelerate [29-31].

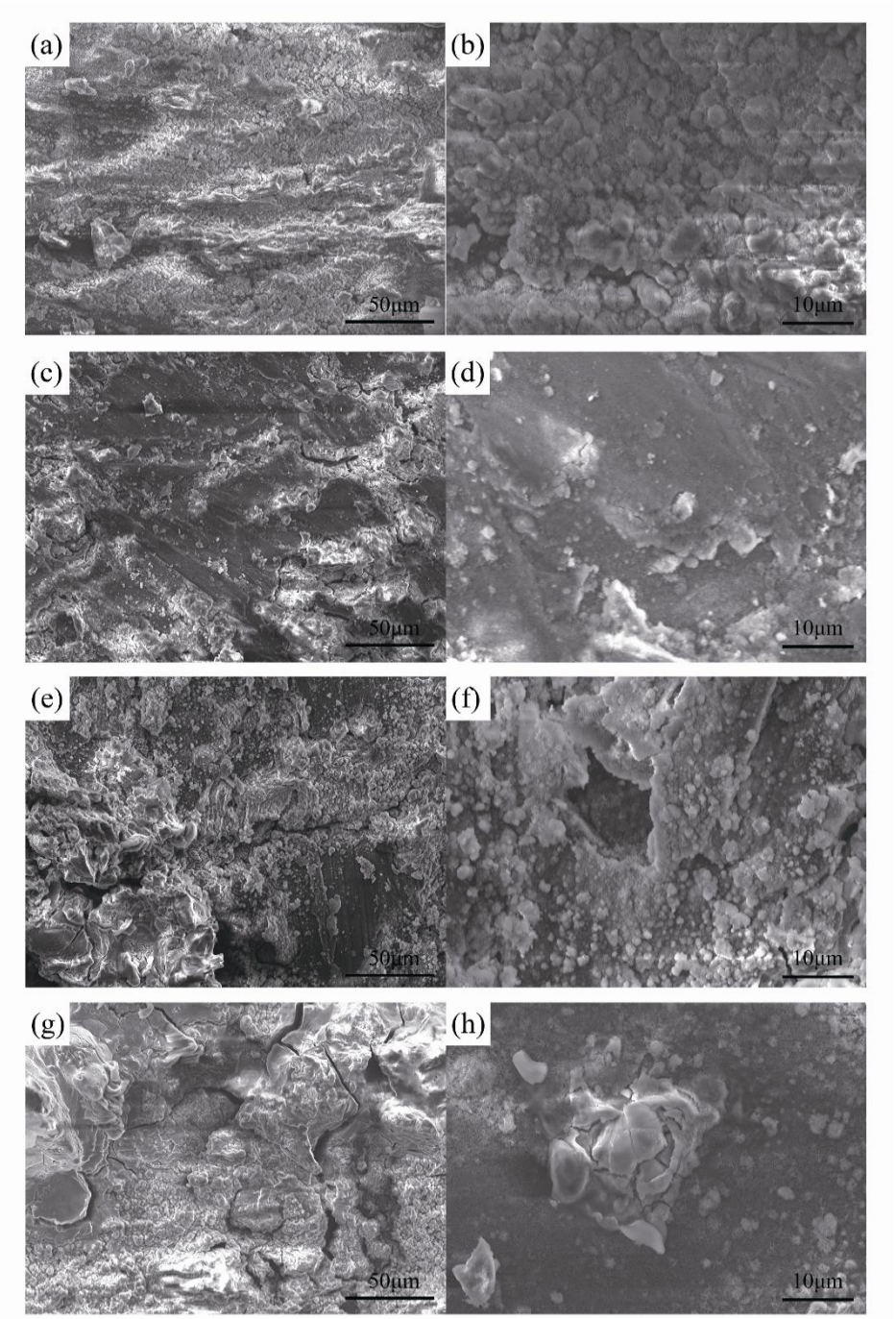

Figure 5. SEM images of the as-rolled Mg-8Li-xAl alloys after hydrogen evolution: (a and b) Mg-8Li; (c and d) Mg-8Li-2Al; (e and f) Mg-8Li-3Al; (g and h) Mg-8Li-4Al.

In the process of the hydrogen evolution of Mg-8Li-xAl alloy in NaCl solution, the H^+ ions in electrolysis in NaCl solution get electrons from MgLi alloy, and hydrogen will be generated. When the MgLi alloy loses electrons, it will generate Mg (OH) 2 precipitation. Because of electrochemical corrosion, the precipitation of Mg (OH) 2 can not prevent further reaction. If Mg alloy is immersed in NaCl solution for a long time, all of them will participate in the reaction to generate precipitation. If the Mg (OH) 2 precipitates are generated in the wet seaside environment, a loose MgO film will be reacted on the alloy surface to retard the corrosion of the alloy. Therefore, how to prepare dense protective film

or coating on the surface of MgLi alloy based on corrosion mechanism will be the key technology to improve the corrosion resistance of MgLi alloy.

To distinguish the corrosion resistance of different alloys more accurately. Potential-dynamic polarization curves of Mg-8Li alloy, Mg-8Li-2Al, Mg-8Li-3Al and Mg-8Li-4Al alloys are presented in Fig. 6. Lower current density in cathodic part than anodic part revealed that the corrosion of Mg-Li or Mg-Li-Al alloys were controlled by the cathodic hydrogen evolution reaction. Obviously, the cathodic current density gradually increased with the enhanced addition of Al element. The lowest and highest rates of cathodic reaction were identified from curves of Mg-8Li and Mg-8Li-4Al alloys respectively. Such an accelerated cathodic current might contribute to more strong galvanic corrosion after addition of Al. In anodic branch, which represented the dissolution of Mg or its alloys, similar trend like cathodic part was observed again. Higher extent of alloying Al caused quicker dissolution, associated with more corrosion damage. In summary, the increased addition of Al deteriorated the corrosion resistance of Mg-Li-Al alloy.[32,33]

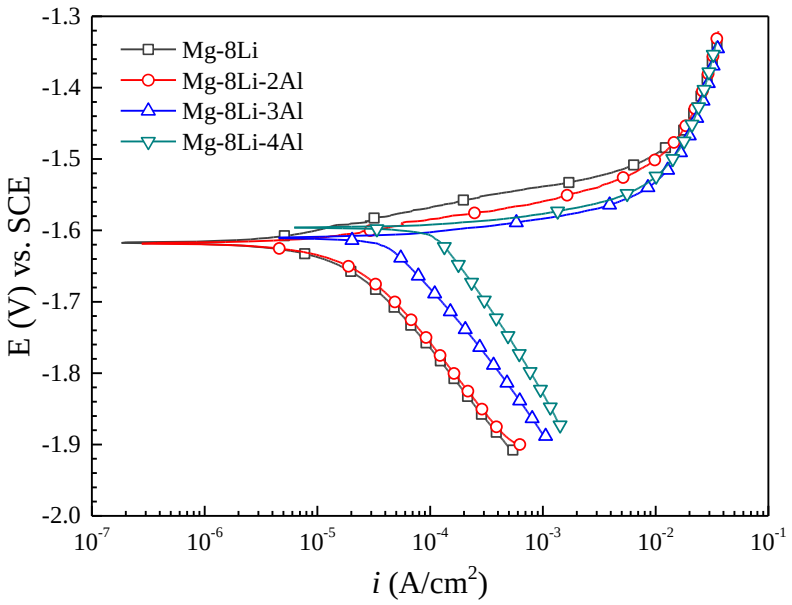

Figure 6. Potentiodynamic polarization curves of Mg-8Li alloy, Mg-8Li-2Al, Mg-8Li-3Al and Mg-8Li-4Al alloys after immersion in 3.5 wt% NaCl solution for 100 min.

Table 1. Electrochemical and corrosion parameters of magnesium in 3.5 wt.% NaCl solution

	E_{corr} (V_{SCE})	I_{corr} (A cm^{-2})
Mg-8Li	-1.624	2.2×10^{-5}
Mg-8Li-2Al	-1.646	3.6×10^{-5}
Mg-8Li-3Al	-1.693	8.2×10^{-5}
Mg-8Li-4Al	-1.726	1.3×10

EIS measurements were carried out in order to further elucidate the Al content dependent electrochemical response of the four alloys tested, and the corresponding Nyquist plots are shown in Fig. 7. Mg-8Li displayed a Nyquist plot with three semi-circles, i.e. A capacitive loop at high frequency, a capacitive loop at medium frequency, and an inductive loop at low frequency. In terms of three Mg-Li-Al alloys, there were a capacitive loop and an inductive loop. Obviously the corrosion resistance gradually decreased with the enhancement of alloying Al. Additionally, it was noted that the inductive loop which could be found in three Mg-Li-Al alloys at low frequency implied the breakdown of corrosion film caused by localized corrosion. The remaining capacitive loop was a mixed response of charge transfer process and partial surface film. The tendency of localized corrosion increased with enhanced Al content. With respect to the Mg-8Li alloy, the far smaller inductive loop meant slight extent of localized corrosion.

Fig.8 illustrates the equivalent circuits to fit the measured EIS results after immersion of 1.5 h. The parameters of the equivalent had the following meanings.

R_s : the resistance of solution between working electrode; Q_f : the constant phase element representing the surface film capacitance; R_f : the surface film resistance; Q_{dl} : the constant phase element related to the double layer capacitance; R_t : the charge transfer resistance; L : breakdown of partial protective film on surface.

Table 1 presents the fitted parameters. According to the fitting results, Mg-8Li alloy showed higher R_t and R_f than others. It indicated a more difficult charge transfer process and the better protective effect of the corrosion film. Comparatively, the lower R_t with increasing Al content of three Mg-Li-Al alloys confirmed the negative effect after introducing alloying Al to corrosion behavior.

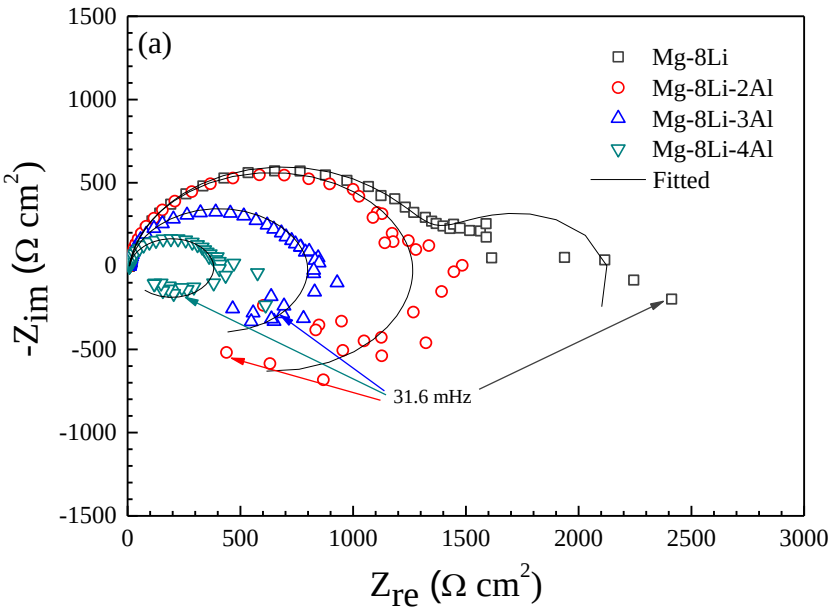

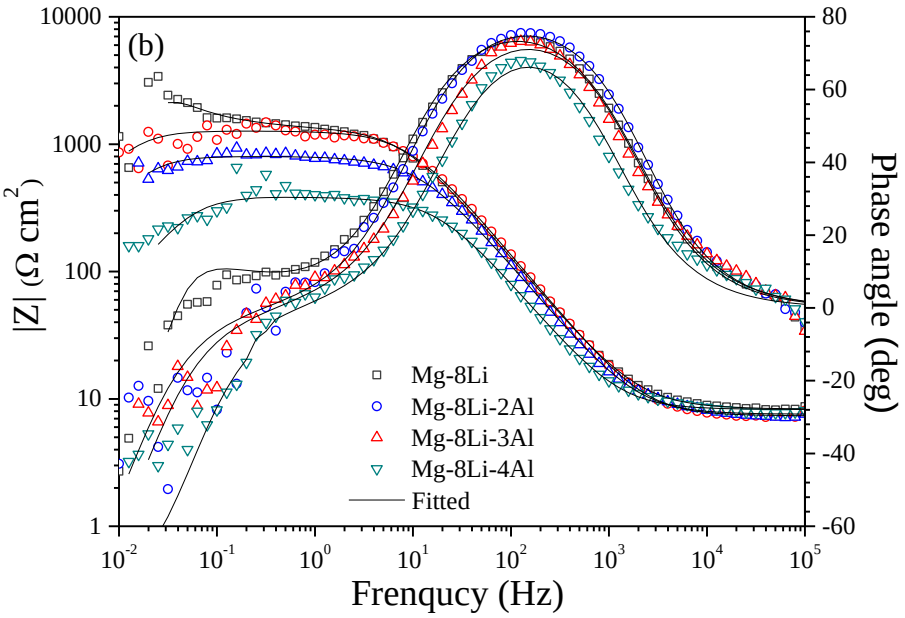

Figure 7. EIS of Mg-8Li alloy, Mg-8Li-2Al, Mg-8Li-3Al and Mg-8Li-4Al alloys after immersion in 3.5 wt% NaCl solution for 100 min: (a) Nyquist and (b) Bode.

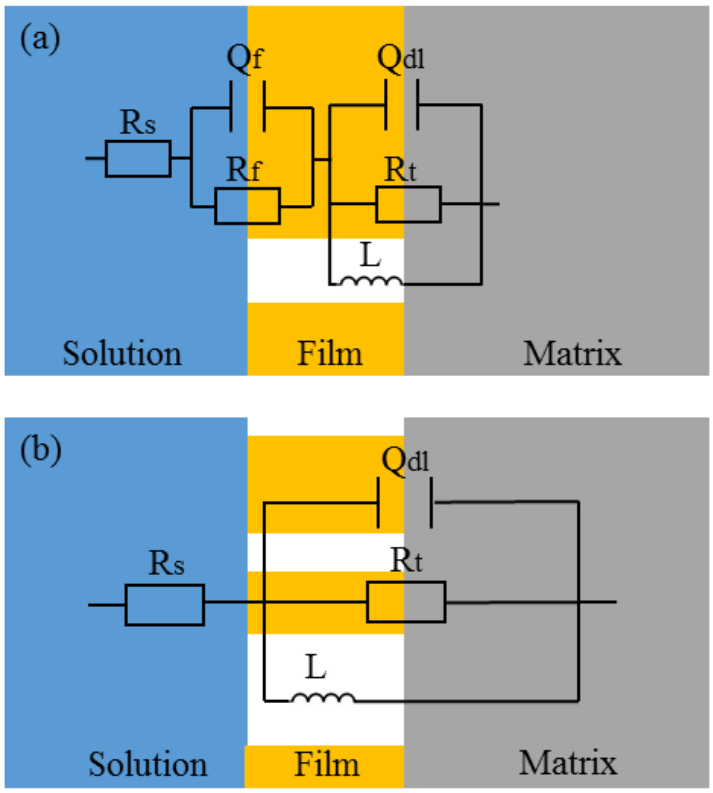

Figure 8. Equivalent circuits of the EIS spectra of: (a) Mg-8Li alloy, (b) Mg-8Li-2Al, Mg-8Li-3Al and Mg-8Li-4Al alloys.

Table 2. Values of the equivalent elements in the equivalent circuits.

	Mg-8Li	Mg-8Li-2Al	Mg-8Li-3Al	Mg-8Li-4Al
R_s (Ω cm^2)	8.28	7.36	7.57	8.25
Q_f (F cm^{-2})	2.40×10^{-3}	/	/	/
n	0.64	/	/	/
R_f (Ω cm^2)	1514	/	/	/
Q_{dl} (F cm^{-2})	2.14×10^{-5}	1.90×10^{-5}	2.54×10^{-5}	3.40×10^{-5}
n	0.92	0.93	0.91	0.92
R_t (Ω cm^2)	1278	1263	795	376
L (H cm^{-2})	4733	1.54×10^{4}	6964	1771

4. CONCLUSIONS

Song et al. reported that grain refinement led to the decrease in corrosion resistance of pure Mg [34] and AZ91D Mg alloy [35] in 3.5 mass%NaCl aqueous solution. In this paper, when the Al content exceeds 3%, the corrosion resistance of Mg-8Li alloy in air can be obviously improved. The addition of Al resulted in more electrochemical corrosion of Mg-8Li alloy in NaCl% solution, which accelerated the rate of hydrogen evolution.With the increase of Al content, AlLi is more and more, and the rate of hydrogen evolution reaction will accelerate. How to prepare dense protective film or coating on the surface of MgLi alloy based on corrosion mechanism will be the key technology to improve the corrosion resistance of MgLi alloy.

ACKNOWLEDGEMENTS
This work was supported by National Natural Science Foundation of China (Nos. 51778088 and 51701029), Chongqing Science Foundation of China (Nos. cstc2017jcyjBX00036 and cstc2016jcyjA0388), Fundamental Research Funds for the Central Universities (Nos. 2018CDQYTM0054 and 106112017CDJXY130002), China (Chongqing) Singapore Post-Doctoral international training exchange program([2017] 78 and [2017] 154).

References

1. A. Atrens, G.-L. Song, M. Liu, Z. Shi, F. Cao and M. S. Dargusch, *Adv. Eng. Mater*., 17 (2015) 400.
2. B. Feng, Y. C. Xin, F. L. Guo, H. H. Yu, Y. Wu and Q. Liu, *Acta Mater*., 120 (2016) 379.
3. G. Zhang, L. Wu, A. Tang, B. Weng, Andrej. Atrens, S. Ma, L. Liu and F. Pan, *RSC Advances*, 8 (2018) 2248.
4. F. Zhang, Z. G. Liu, R. C. Zeng, S. Q. Li, H. Z. Cui, L. Song and E. H. Han, *Surf. Coat. Technol*., 258 (2014) 1152.
5. J. K. Lin, J. Y. Uan, C. P. Wu and H. H. Huang, *J. Mater. Chem*., 21 (2011) 5011
6. L. Wu, Z. Zheng, F. Pan, A. Tang, G. Zhang and L. Liu, *Int. J. Electrochem. Sci.,* 12 (2017) 6352.
7. M. Bamberger and G. Dehm, *Annu. Rev. Mater. Sci*. 38 (2008) 505.
8. B.L. Mordike and T. Ebert, *Mater. Sci. Eng*., A 302 (2001) 37.
9. B. S. Liu, Y. F. Kuang, Y. S. Chai, D. Q. Fang, M. G. Zhang， Y. H. Wei and J. Magnes. *Alloy*, 4 (2016) 220.

10. A. Atrens, G. L. Song, F. Cao, Z. Shi and P. K. Bowen, *J. Magnes. Alloy*, 1 (2013) 177.
11. A. Atrens, M. Liu and N. I. Z. Abidin, *Mater. Sci. Eng*., B, 176 (2011) 1609.
12. D. K. Ivanou, M. Starykevich, A. D. Lisenkov, M. L. Zheludkevich, H. B. Xue, S. V. Lamaka and M. G. S. Ferreira, *Corros. Sci*., 73 (2013) 300.
13. S. A. Salman, R. Mori, R. Ichino and M. Okido, *Mater. Trans*., 51 (2010) 1109.
14. X. B. Chen, N. Birbilis and T. B. Abbott, *Corrosion*, 67 (2011) 035005.
15. R.G.Song, L.Chen and H.Lu, *Surf Eng*., 33 (2017) 451.
16. F.Zhang, C.Zhang and S.Liang, *Nonferrous Met. Soc. China*., 25 (2015) 3498.
17. R.G.Song, L.Chen and H.Lu, *Surf. Eng*., 33 (2017) 451.
18. F.Zhang, C.Zhang and S.Liang, *Trans. Nonferrous Met. Soc. China*. 25 (2015) 3498.
19. Y. Zeng, B. Jiang, R. H. Li, J. J. He, X. S. Xia and F. S. Pan, *Mater. Sci. Eng*., A 631 (2015) 189.
20. D. K. Xu, B. J. Wang and Z. J. Wang, *Mater. Des*., 69 (2015) 124.
21. X. Y. Guo, R. Z. Wu and L. J. Huang, *Mater. Sci. Eng*. A, 53 (2014) 528.
22. F. R. Cao, F. Xia, H. L. Hou, H. Ding and Z. Q. Li, *Mater. Sci. Eng*. A, 637 (2015) 89.
23. Z.L.Zhao, X.G.Xing, Y.Luo, Y.D.Wang and W.Liang, *J. Iron Steel Res. Int.*. 24 (2017) 426.
24. Z.Zhao, Z.Sun, W.Liang, Y.Wang and L.Bian, *Mater,Sci.Eng*.A. 702 (2017) 206.
25. W.Xu, N.Birbilis, G.Sha, Y.Wang and JE.Daniels, *Nat. Mater.*. 12 (2015) 1229.
26. G. Park, J. Kim, H. Park, Y. Kim, H. Jeong, N. Lee, Y. Seo, J. Suh, H. Son, W. Wang, J. Park and K. Kim, *J. Alloy. Compd*. 680 (2016) 116.
27. L.Wu, D.Yang, G.Zhang, Z.Zhang, S.Zhang, A.Tang and F.Pan, *Appl. Surf. Sci.*, 431 (2018) 177.
28. L.Wu, G.Zhang, A.Tang, Y.Liu and A.Atrens, *J. Electrochem. Soc*., 167 (2017) 339.
29. G.Zhang, L.Wu, A.Tang, Y.Ma, G.Song, D.Zheng, B.Jiang, A.Atrens and F.Pan. *Corrosion Sci*., 139 (2018) 370.
30. G.Zhang, L.Wu, A.Tang, X.Chen, Y.Ma, Y.Long, P.Peng, X.Ding, H.Pan, F.Pan. *Corrosion Sci*., 456 (2018) 419.
31. G.Zhang, L.Wu, A.Tang, H.Pan, Y.Ma, Q.Zhan, Q.Tan, F.Pan, Andrej Atrens. *J. Electrochem. Soc*., 165 (2018) 317.
32. Rad, H. R. B., Idris, M. H., Kadir, M. R. A. and Farahany, S. *Mater. Des*., 33 (2012) 88.
33. Q.Xiang, B.Jiang, Y.Zhang, X.Chen, J.Song, J.Xu, L.Fang and F.Pan. *Corrosion Sci*., 119 (2017) 14.
34. D. Song, A.B. Ma, J.H. Jiang, P.H. Lin, D.H. Yang and J.F. Fan, *Corros. Sci*. 52 (2010) 481.
35. D. Song, A.B. Ma, J.H. Jiang, P.H. Lin, D.H. Yang and J.F. Fan, *Corros. Sci*. 53 (2011) 362.